High-resolution study of the magnetic-field effect on the ^4E state of Mn^{2+} in cubic ZnS by laser spectroscopy

R. Parrot
Université des Antilles Guyane, Institut Universitaire de Formation des Maîtres et Faculté de Technologie de la Guyane, Boîte Postale, 792, 97337 Cayenne Cedex, French Guyana

D. Boulanger
Université de Paris–Sud, Laboratoire d'Informatique Maîtrise de Sciences Physiques, Bâtiment 479, 91405 Orsay Cedex, France

B. Litzenburger, U. W. Pohl, and H. E. Gumlich
Technical University of Berlin, Institute of Solid State Physics, Hardenbergstrasse 36, D-10626 Berlin, Germany

M. N. Diarra
Université de Dakar, Département de Physique, Dakar-Fann, Sénégal
(Received 13 February 1995)

The influence of a magnetic field on the fine-structure lines of the ^4E state of Mn^{2+} in pure cubic ZnS has been studied up to 5 T by using polarization-modulated laser spectroscopy. Very detailed analyses of polarized excitation spectra of the transitions $^6A_1 \rightarrow {}^4E$ show that all authorized transitions have been observed between the Zeeman sublevels of the Kramers doublets Γ_6 (^4E), Γ_7 (^4E), and spin quartet Γ_8 (^4E) and the levels $^6A_1$ ($M_S=-\frac{5}{2}$) and $^6A_1$ ($M_S=-\frac{3}{2}$) of the fundamental state. Many other transitions from the levels $^6A_1$ ($M_S=-\frac{1}{2}$), $^6A_1$ ($M_S=+\frac{1}{2}$), $^6A_1$ ($M_S=+\frac{3}{2}$), and $^6A_1$ ($M_S=+\frac{5}{2}$) have been observed at low magnetic field. It is shown that the Zeeman effect on the levels Γ_6, Γ_7, and Γ_8 is correctly described by the Zeeman Hamiltonian $g_e\mu_B\mathbf{H}\cdot\mathbf{S}$, and that the contribution of the term in $\mu_B\mathbf{L}\cdot\mathbf{H}$, which appears in second-order perturbation schemes involving the spin-orbit interaction, is negligible.

I. INTRODUCTION

Very detailed experimental and theoretical studies have long been performed on the electronic and vibronic structures of the fundamental and excited states of d^n ions in crystals and molecules.[1] In the case of the d^5 ions, the studies have been devoted to an overall analysis of the energy levels in the crystal-field model[2,3] or covalent models,[4–6] and also to detailed analyses of the fine-structure pattern associated with the excited states at lower energy, as the fluorescent level $^4T_1(G)$ and levels $^4T_2(G)$ and $^4E(G)$ (see Fig. 1).

In the case of Mn^{2+} in II-VI compounds such as ZnS (Refs. 7–9) and ZnSe,[8] and III-V compounds such as GaP,[10] the structure of the fluorescent orbital triplet state $^4T_1(G)$ has been interpreted in terms of a coupling to vibrational modes of symmetry E, the coupling being strong enough to quench the first-order spin-orbit interaction and the coupling to internal strains or stress-induced uniaxial strains of symmetry T_2 almost completely. In ZnS and ZnSe, the fine-structure pattern of the next excited state $^4T_2(G)$ has been analyzed in terms of an intermediate coupling to E modes, leading to a partial quenching of the first-order spin-orbit interaction and a selective intensity transfer from the fundamental vibronic states to excited vibronic states.[11]

Concerning the third excited state ^4E of Mn^{2+} in cubic symmetry, the fine-structure pattern consists of three lines associated with two Kramers doublets Γ_6 and Γ_7 and a quartet Γ_8. This structure was analyzed in terms of a second-order spin-orbit interaction.[12] Since then, detailed studies have shown that higher-order spin-orbit interactions intervene, and that the splitting of the ^4E state depends on the nature of the ligands and on the strength of the Jahn-Teller coupling to E modes, as has been shown from a theoretical study of the splitting of the ^4E state in ZnSe which is less than half the splitting observed in ZnS.[13]

Although the electronic and vibronic structures of the $^4E(G)$ of Mn^{2+} in cubic symmetry have been correctly analyzed in great detail by using models involving the spin-orbit interaction of the d electrons of Mn^{2+} and the dynamical Jahn-Teller effect, the electronic structure of the $^4E(G)$ states remains very puzzling in noncubic symmetries induced, for example, by internal strains in nearly tetrahedral clusters MnX_4(X:S,Se,Cl,Br) or by stress-induced uniaxial strains on tetrahedral clusters MnS_4 and $MnSe_4$.[14] More precisely, the observed splitting of the state $\Gamma_8(^4E)$ and the shifts of the states $\Gamma_6(^4E)$ and $\Gamma_7(^4E)$ in nearly cubic symmetry can be mimicked by a first-order coupling to static E strains, the coupling to T_2 strains being negligible. This result is in contradiction with the predictions of the crystal-field model restricted to the configuration d^5, because in this model a first-order coupling to T_2 strains is forbidden by symmetry, and a first-order coupling to E strains allowed by symmetry is forbidden by seniority, since for half-filled shell systems the matrix elements of single-electron even opera-

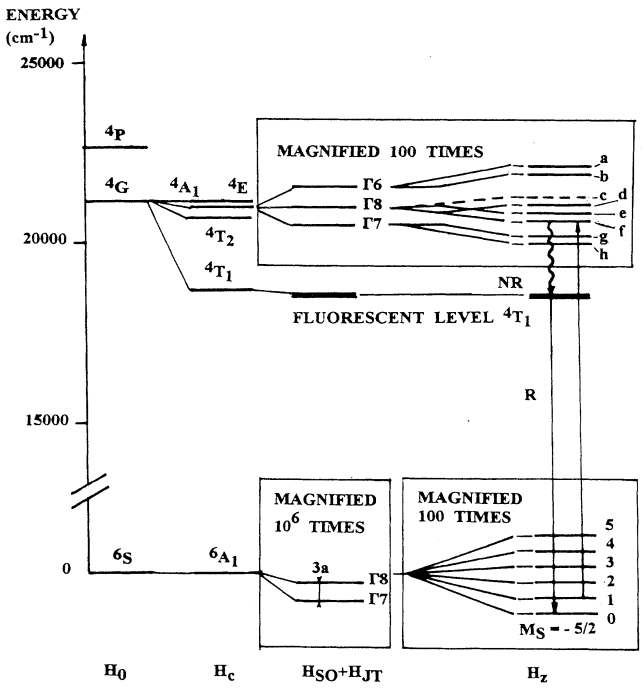

FIG. 1. Lowest-energy levels of Mn^{2+} in ZnS as given by the free-ion Hamiltonian H_0, the cubic crystal field H_c, the spin-orbit and Jahn-Teller interactions $H_{so}+H_{JT}$, and the Zeeman Hamiltonian H_Z. The influence of the magnetic field is given for $\mathbf{H}\|[111]$. For convenience the eight Zeeman sublevels associated with the ^4E state are simply labeled $a,b,\ldots,h$ and the Zeeman sublevels SM_S associated with the fundamental states $\Gamma_7(^6A_1)$ and $\Gamma_8(^6A_1)$ are labeled $0,1,..,5$. The transition represented is the transition $f1$, the arrows NR and R, respectively, represent the nonradiative transitions from level f to the fluorescent level $^4T_1$ and the radiative transition from state $^4T_1$ to the fundamental state. Level c is represented by a broken line because no transition to this level has been observed.

tors are zero when they are diagonal in the seniority,[15] so that the matrix element $\langle {}^4E(\frac{4}{5}G)|H_E|{}^4E(\frac{4}{5}G)\rangle$ is zero. (The spectroscopic term is written in detail as ${}^{2S+1}_{v}L$, v being the seniority number and H_E an even operator of E symmetry describing, for example, the coupling to E strains). Second-order perturbation schemes predict a linear coupling to T_2 strains and a quadratic coupling to E strains, a result which is in contradiction with experiments. As has been shown in the crystal-field model, high-order perturbation schemes involving spin-orbit interaction and configuration interactions contribute to a linear coupling of the ^4E state to E strains. Moreover, just as it is difficult to justify theoretically the observed linear coupling to E strains, it is likewise difficult to justify the nonobservation of a coupling to static T_2 strains, since the strength of the coupling to E modes does not seem to be strong enough to completely quench the effect of the coupling to T_2 strains.

Among the very few studies of the magnetic-field effect on the excited states of Mn^{2+}, we can cite those of Fournier, Boccara, and Rivoal[7] on the fluorescent state of Mn^{2+} in ZnS; Landi, Deville, and Ranvaud[16] on the state $^4T_2$ at lower energy of Mn^{2+} in ZnS, and Hofman, Anderson, and Weber[10] on the fluorescent state of Mn^{2+} in GaP. Concerning the ^4E state, an experiment performed long ago did not permit a detailed interpretation of the Zeeman effect in this state due to a limited resolution of an experimental setup of only 10 cm^{-1}.[17] An experimental study with improved experimental conditions has been performed more recently, but a definite interpretation of the Zeeman effect was not given.[18]

The aim of this work was to analyze the Zeeman effect of the $^4E(G)$ state of Mn^{2+} in ZnS at high resolution in selected pure cubic crystals presenting very sharp fine structure lines, and then to determine the contributions of the terms in $\mathbf{S}\cdot\mathbf{H}$ and $\mathbf{L}\cdot\mathbf{H}$ which appear in the Zeeman Hamiltonian and, finally, to detect an eventual coupling between the states $\Gamma_8(^4E)$ and $\Gamma_8(^4A_1)$ which could give an indication on the energy of this state that, to our knowledge, has never been unambiguously observed in experimental spectra.

In Sec. II, the criteria governing the selection of crystals as well as the experimental method of polarization-modulated excitation spectroscopy are given, then polarized experimental spectra are presented for magnetic fields varying up to 5 T. The Zeeman splitting of the ^4E state is deduced from the energies of transitions from Zeeman components of the fundamental state to the Zeeman components of the ^4E state.

The theoretical model is presented in Sec. III. A resume of the structure of the ^4E state in zero magnetic field is presented, then a theoretical analysis is made of the Zeeman Hamiltonian for the ^4E state and of the spin Hamiltonian of the fundamental state $^6A_1$. Finally, the theoretical energy levels and polarization effects are presented.

In Sec. IV, a very detailed comparison is made of the experimental and theoretical spectra. It is shown that the experimental spectra are correctly described by taking into account the term in $\mathbf{H}\cdot\mathbf{S}$ of the Zeeman Hamiltonian, the influence of the term in $\mathbf{L}\cdot\mathbf{H}$ being negligible.

II. EXPERIMENTS

A. Samples and apparatus

The experiments were performed on ZnS:Mn crystals grown at the Institute of Solid State Physics of the Technical University of Berlin. Great care was given to the selection of the crystals used in Zeeman experiments. Since the Zeeman spectra of the level ^4E were expected to be complex enough, even in the simplest case of isolated Mn^{2+} ions in cubic sites, crystals showing stacking faults,[19] Mn-Mn pair spectra,[20] or large internal strains were rejected.

For the selected crystals, no fine-structure line due to Mn^{2+} centers in stacking faults has been observed in the excitation spectra from the fundamental state to the excited states $^4T_2$ and ^4E or in the emission spectra $^4T_1\rightarrow{}^6A_1$, thus demonstrating that the crystals are pure-

ly cubic. Furthermore, the concentration of Mn^{2+} ions was chosen to be as low as 10^{-4} mole fraction, so that no fine structure line due to Mn-Mn pairs was observed near level $^4T_1$ or levels $^4T_2$ and ^4E. Finally, due to very low internal strains, fine-structure lines associated with the level ^4E studied here and also with fluorescent level $^4T_1$ and excited level $^4T_2$ were among the most sharply observed until now.

The excitation spectra were obtained by using a laser system (Lambda Physik) consisting of a XeCl* excimer laser pumping a dye laser. The linewidth of the laser system was approximately 0.4 cm^{-1}. The emission light was selected by a monochromator centered at 17 240 cm^{-1} (the maximum of the emission band).

Polarized excitation spectroscopy was performed by using a modulation technique similar to magnetic circular dichroism used in absorption spectroscopy.[21,22] The principle of polarized excitation spectroscopy is as follows: the pulsed laser is synchronized to the phase of a stress modulator, which transforms the excitation light into alternating left and right circularly polarized light. By recording the pulsed emission light with a gated photon-counting system, the spectra σ^+ and σ^- are recorded almost simultaneously. In our experiments, the degree of polarization was better than 95%.

The magnetic field was given by a superconducting split coil operating up to 5 T, and the homogeneity of the magnetic field was better than 1% in the volume of the samples. The experiments were performed with **H** parallel to a crystallographic axis [111], the light propagating along the same axis. All experiments were performed with the crystal immersed in pumped liquid helium. The typical temperature was chosen to be 2.0±0.1 K.

B. Experimental spectra

The experimental spectra corresponding to the polarizations σ^+ and σ^- are given in Fig. 2. *It must be noted that the experimental linewidths of 0.4 cm^{-1} are limited by the resolution of the dye laser and not by the inhomogeneous line broadening.*

For $B=0$, three transitions $^6A_1 \rightarrow \Gamma_6(^4E)$, $^6A_1 \rightarrow \Gamma_7(^4E)$, and $^6A_1 \rightarrow \Gamma_8(^4E)$ are very well resolved. The splittings are $W(\Gamma_6)-W(\Gamma_8)=4.85$ cm^{-1} and $W(\Gamma_8)-W(\Gamma_7)=4.25$ cm^{-1}.

For $B=0.25$ T, splittings of the fine-structure lines clearly appear for the polarizations σ^+ and σ^-. In fact, numerous transitions from the six fundamental states $^6A_1$ ($M_S=-\frac{5}{2},-\frac{3}{2},\ldots,+\frac{5}{2}$) to the eight components of the ^4E state contribute to the spectra.

For $B=0.5$, 0.75, and 1 T, numerous lines appear in the experimental spectra. For $B=1$ T, three prominent lines clearly appear for the polarization σ^+.

For B increasing from 1 to 5 T, the energy separation between the three prominent lines appearing for polarization σ^+ increases. For $B=3$, 4, and 5 T, one intense line appears for the polarization σ^+. No clear overall feature is observed for the polarization σ^-.

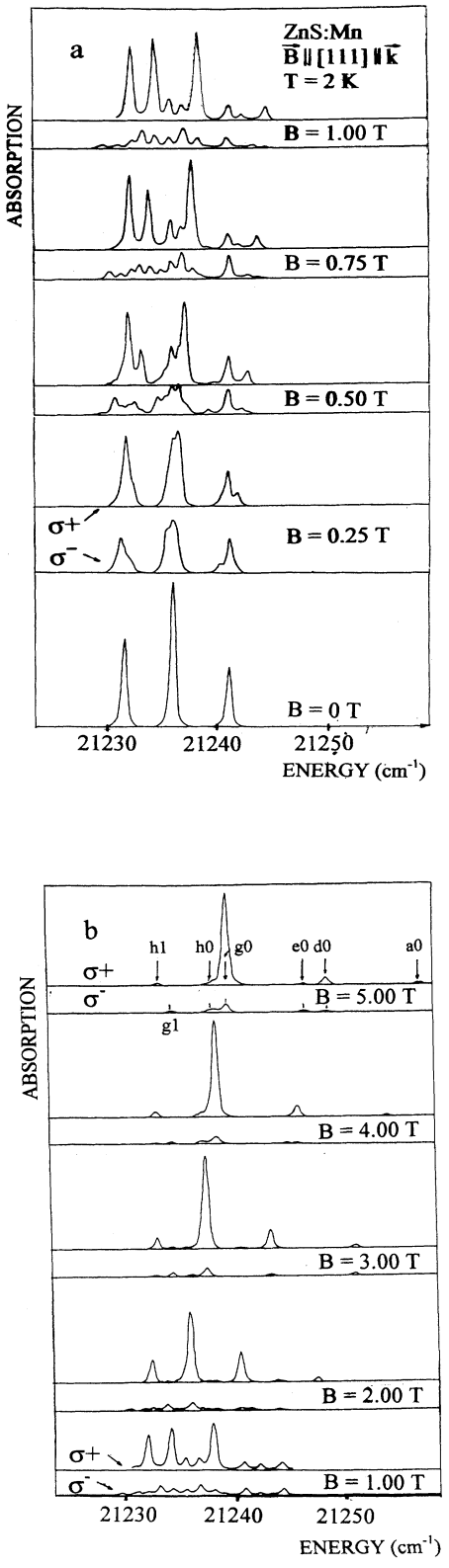

FIG. 2. Polarized excitation spectra of the transition $^6A_1 \rightarrow {}^4E(G)$ for B extending from 0 to 5 T. The spectra corresponding to the polarization σ^+ and σ^- are represented. In (b) the scaling is half that chosen in (a). The spectra obtained for $B=1$ and 5 T are interpreted in Sec. IV.

C. Energy levels

The energy levels are presented in Fig. 3. By considering first the level Γ_7 at lower energy, three groups of two lines (which will be associated with the transitions $g0,h0,g1,h1$, and $g2,h2$) clearly appear for B extending from 0 to 4 and 5 T. Given the value of the spacing between the three groups of lines and the fact that the spacing is linear in B, the two lines of the group at higher energy can safely be associated to the transitions $g0$ and $h0$ which are transitions between the two Zeeman states Γ_7 and the fundamental state ${}^6A_1$ ($S=\frac{5}{2}, M_S=-\frac{5}{2}$), the two other groups of two lines are associated to the transitions $g1$, $h1$ and $g2,h2$ corresponding to the transitions ${}^6A_1$ ($M_S=-\frac{3}{2}$)$\rightarrow\Gamma_7$ and ${}^6A_1(M_S=-\frac{1}{2})\rightarrow\Gamma_7$. Other lines appearing for $B<2$ T are associated with transitions ${}^6A_1(M_S=+\frac{1}{2}, +\frac{3}{2}$, and $+\frac{5}{2})\rightarrow\Gamma_7$.

The splitting of state Γ_6 can be relatively easily analyzed in terms of transitions from the fundamental state. Two groups of two lines appearing at higher energy correspond to transitions $a0,b0$ and $a1,b1$; that is, transitions ${}^6A_1$ ($M_S=-\frac{5}{2}$ and $-\frac{3}{2}$)$\rightarrow\Gamma_6$. As for the level Γ_7, other lines appearing when $B<2$ T are associated to transitions ${}^6A_1$ ($M_S=-\frac{1}{2}, +\frac{1}{2}$, etc)$\rightarrow\Gamma_6$.

State Γ_8 was by far the most difficult to analyze, since numerous lines can be associated with the states Γ_6 or Γ_7, and since no group of lines separated by $\mu_B g_e H$, which is the splitting of two consecutive Zeeman levels in the fundamental state, appeared in the spectra. In fact, the lines associated to the transitions ${}^6A_1$ ($M_S=-\frac{5}{2}$ and $-\frac{3}{2}$)$\rightarrow\Gamma_8$ will be determined in Sec. IV by comparing the experimental and theoretical spectra.

D. Magnetic-field-induced splitting of the ${}^4E$ state

The experimental results concerning the magnetic-field-induced splitting of the states Γ_6, Γ_7, and Γ_8 are given in Fig. 4. The splittings have been obtained by adding the relevant shift $\mu_B g_e H M_S$ of the fundamental state to the energies of the experimental transitions.

For state Γ_6, transitions ${}^6A_1$ ($M_S=-\frac{5}{2}, -\frac{3}{2}, -\frac{1}{2}$, and $+\frac{1}{2}$)$\rightarrow\Gamma_6$ have been analyzed. It must be noted that after adding $\mu_B g_e H M_S$, all analyzed lines appear on the energy-level diagram with a precision of 0.1 cm^{-1}.

For the state Γ_7, transitions ${}^6A_1$ ($M_S=-\frac{5}{2}$ and $-\frac{3}{2}$)$\rightarrow\Gamma_7$ are clearly observed. Several transitions corresponding to $M_S=-\frac{1}{2}$ and $+\frac{1}{2}$ have been observed for $B<2$ T. For $B<1$ T, several transitions have been associated with $M_S=+\frac{3}{2}$.

For the state Γ_8, the two lines which are superposed for $B=3$ T correspond to transitions ${}^6A_1$ ($M_S=-\frac{5}{2}$)$\rightarrow\Gamma_8$.

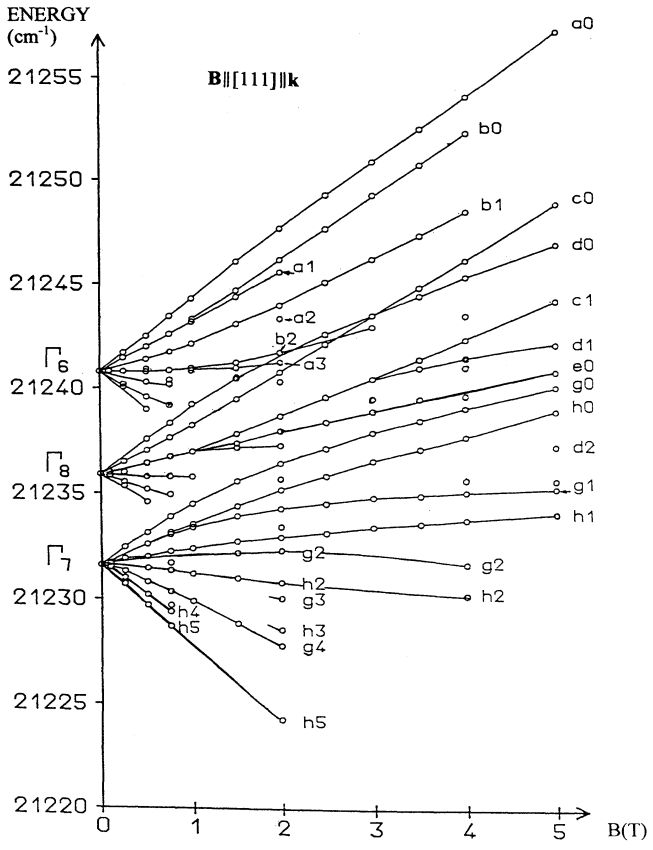

FIG. 3. Experimental energy levels in terms of the magnetic field. The indexation of the lines associated with states Γ_6 and Γ_7 is valid for B extending from 0 to 5 T. For state Γ_8, the indexation of the lines for B extending from 0 to 4 T cannot be represented simply, since, as shown in Sec. IV, several transitions can contribute to a given excitation line.

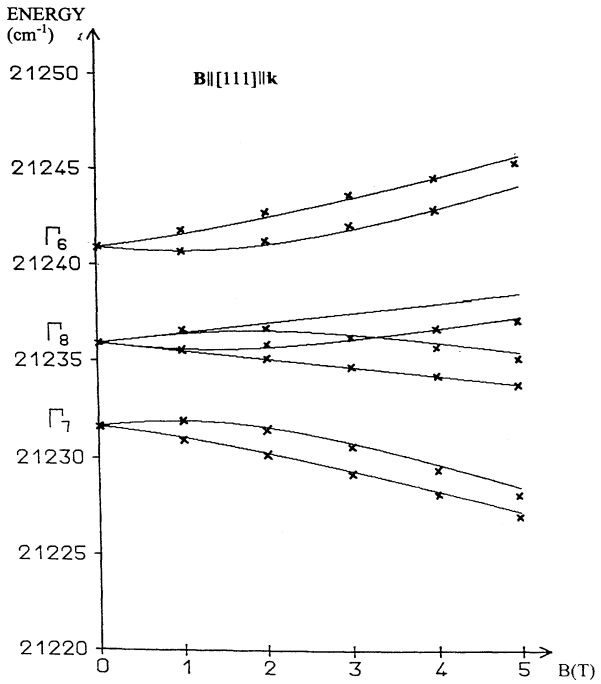

FIG. 4. Theoretical (solid line) and experimental splittings (crosses) of the states Γ_6, Γ_7, and Γ_8, as deduced from the energies of the transitions ${}^6A_1$ ($M_S=-\frac{5}{2}, -\frac{3}{2}, -\frac{1}{2}, +\frac{1}{2}, +\frac{3}{2}, +\frac{5}{2}$)$\rightarrow\Gamma_6\Gamma_7,\Gamma_8$. No transition to level c has been observed.

III. THEORETICAL MODEL

A. Structure of the ^4E state in zero magnetic field

We will briefly recall here the structure of the ^4E state at lower energy of Mn^{2+} in tetrahedral symmetry as given by previous experiments and theoretical models.[13] In a crystal-field model, the general Hamiltonian governing the energy levels of d ions in cubic symmetry can be written as

$$H=H_0+H_{\rm CUB}+H_{\rm SO}+H_{\rm SS}+H_{\rm EL}+H_{\rm K}+H_{\rm JT}+H_{\rm EXT} ,$$

where H_0 is the free ion Hamiltonian, $H_{\rm CUB}$ is the Hamiltonian in a cubic field, $H_{\rm so}$ and $H_{\rm ss}$ represent the spin-orbit and spin-spin interactions, respectively. $H_{\rm EL}$ and $H_{\rm K}$ are the elastic and kinetic energies associated to the effective vibrational modes, and $H_{\rm JT}$ is the Jahn-Teller Hamiltonian describing the electron-nuclear interaction. $H_{\rm EXT}$ corresponds to external perturbation effects as the magnetic-field effect which will be considered in Sec. III B, the uniaxial stress effect, the electric field effect, etc.

When analyzing the energy levels of d^5 ions due to $H_0+H_{\rm CUB}$ in a crystal-field model, it appears that the levels $^4E(G)$ and $^4A_1(G)$ are degenerate, this result is in disagreement with experimental results which show that the experimental spectra are to be associated to the three fine-structure states Γ_6, Γ_7, and Γ_8 of the ^4E state, the state $\Gamma_8(^4A_1)$ not being strongly mixed to the ^4E state. A covalent model has long been proposed by Koide and Pryce[4] to show that covalency can lift the degeneracy of the states ^4E and $^4A_1$. To our knowledge, this was the first indication showing that the crystal-field Hamiltonian $H_{\rm CUB}$ was to be considered with caution.

The splitting of the ^4E state due to the spin-orbit interaction $H_{\rm so}$ is given primarily by a second-order spin-orbit coupling between the ^4E state and the states $^4T_1$, $^4T_2$, $^2T_1$, and $^2T_2$ of the configuration d^5. The energy levels Γ_6, Γ_7, and Γ_8 are given, in Griffith's notation,[23] by

$$W(t\tau)=\sum_{Sh'J'}\frac{|\langle {}^4Et\tau|H_{\rm so}|S'h'J't\tau\rangle|^2}{W(^4E)-W(S'h')} ,$$

with $t\tau=\Gamma_6$, Γ_7, or Γ_8, with $S'h'={}^4T_1$, $^4T_2$, $^2T_1$, and $^2T_2$. Explicitly, we obtain three equidistant fine-structure lines with $W(\Gamma_6)-W(\Gamma_8)=W(\Gamma_8)-W(\Gamma_7)$, and

$$W(\Gamma_6)-W(\Gamma_8)=\tfrac{1}{30}\{^4T_2\}+\tfrac{1}{30}\{^4T_1\}+\tfrac{1}{24}\{^2T_2\}+\tfrac{1}{24}\{^2T_1\} ,$$

the reduced matrix elements $\{S'h'\}$ being defined by

$$\{S'h'\}=\sum_i\frac{1}{W(^4E)-W(S'h')_i}\times\langle {}^4E\|H_{\rm so}\|(S'h')_i\rangle\times\langle (S'h')_i\|H_{\rm so}\|{}^4E\rangle ,$$

with $S'h'={}^4T_1$, $^4T_2$, $^2T_1$, and $^2T_2$.

In the case of Mn^{2+} in ZnS, the computed splitting $W(\Gamma_6)-W(\Gamma_8)$ was found to be 9.2 cm^{-1}, twice as large as the experimental splitting. The contribution of the spin-spin interaction $H_{\rm ss}$ was 2.6 cm^{-1}.

Figure 2(a) shows that fine-structure lines are not strictly equidistant; in fact, $W(\Gamma_6)-W(\Gamma_8)=4.85$ cm^{-1} and $W(\Gamma_8)-W(\Gamma_7)=4.25$ cm^{-1}. A refined model for the ^4E state has been proposed which shows that fourth-order perturbation schemes involving the spin-orbit interaction between states $\Gamma_8(^4E)$ and $\Gamma_8(^4A_1)$, and the orbital triplet states $^2T_1$ and $^4T_1$ of configuration d^5 can shift state $\Gamma_8(^4E)$. Explicitly, shift $\Delta\Gamma_8(^4E)$ is given by

$$\Delta\Gamma_8(^4E)=\frac{1}{W(^4A_1)-W(^4E)}\times\sum_i(\tfrac{1}{450})\{\{^4T_{1i}\}_{^4E}\{^4T_{1i}\}\}_{^4A_1}+\tfrac{1}{288}\{\{^2T_{1i}\}_{^4E}\{^2T_{1i}\}\}_{^4A_1} ,$$

the reduced matrix element $\{S'h'\}_{Sh}$ being defined, in Griffith's notation, by

$$\{S'h'\}_{Sh}=\sum_i\frac{1}{W(Sh)-W(S'h')i}\times\langle Sh\|H_{\rm so}\|(S'h')i\rangle\times\langle (S'h')i\|H_{\rm so}\|Sh\rangle$$

with $S'h'={}^2T_1$ and $^4T_1$ for Mn^{2+} in ZnS. $\Delta\Gamma_8(^4E)$ was found to be 0.5 cm^{-1}, in good agreement with the experimental shift of 0.3 cm^{-1}.

Concerning the dipole strength, which will be considered in detail in Sec. III C, it has been shown that in tetrahedral symmetry, the relative electric dipole strengths (RDS) are[12]

$$\sigma[^6A_1\rightarrow\Gamma_7(^4E)]=3 ,$$

$$\sigma[^6A_1\rightarrow\Gamma_8(^4E)]=5 ,$$

and

$$\sigma[^6A_1\rightarrow\Gamma_6(^4E)]=2 .$$

Figure 2(a) shows that the experimental and theoretical dipole strengths are in excellent agreement.

B. Magnetic-field effect on states ^4E and $^6A_1$

The Zeeman Hamiltonian is

$$H_Z=\mu_B(\mathbf{L}+g_e\mathbf{S})\cdot\mathbf{H} ,$$

μ_B being the Bohr magneton, g_e the Lande factor of the electron ($g_e=2.0023$),and $\mathbf{H}$ the applied magnetic field.

As shown by symmetry considerations, the matrix elements $\langle {}^4Et\tau|\mathbf{L}\cdot\mathbf{H}|{}^4Et'\tau'\rangle$ are zero, so that the Zeeman effect is primarily due to the term in $\mathbf{S}\cdot\mathbf{H}$.

The calculations have been performed in T_d^*. The basis functions are those given by Griffith,[24] and correspond to an axis system whose vectors are parallel to the cubic axes [100], [010], and [001]. The matrix for $\mathbf{S}\cdot\mathbf{H}$ has been calculated in terms of H_Z, $H+=H_x+iH_y$, and $H_-=H_x-iH_y$. The energy levels are given in Fig. 5 for $\mathbf{H}\|$ [111].

A perturbation method for degenerate states has been used to determine the initial linear splitting of the levels Γ_6, Γ_7, and Γ_8. It can be shown that these levels split following the relations $\Delta W(\Gamma_6)=\Delta W(\Gamma_7)=\Delta W(\Gamma_8)=\pm\mu_B H$. The perturbation is valid when the splitting is much less than the energy separation between the states in zero magnetic field; that is, $\Delta W \ll 4\ \mathrm{cm}^{-1}$.

The contribution of the terms in $\mathbf{L}\cdot\mathbf{H}$ to the Zeeman effect is given by a second-order perturbation scheme. Since in symmetry T_d a state ^4E is coupled by the operator $\mathbf{L}$ to the states $^4T_{1i}$ and $^4T_{2i}$ ($i=1$, 2, and 3), the relevant matrix elements in T_d^* are

$$\sum_{ShJ}\frac{1}{W(^4E)-W(Sh)}(\langle {}^4Et\tau|\mu_B\mathbf{L}\cdot\mathbf{H}|ShJt'\tau'\rangle\langle ShJt'\tau'|H_{so}|{}^4Et'\tau'\rangle+\text{c.c.})$$

The influence of a magnetic field on the fundamental state $^6A_1$ of a d^5 ion in cubic symmetry is given by the spin Hamiltonian

$$H_S=\mu_B\mathbf{S}g\mathbf{H}+\mathbf{S}A\mathbf{I}+\gamma\mathbf{H}\cdot\mathbf{I}$$
$$+(a/6)[S_x^4+S_y^4+S_z^4-\tfrac{1}{5}S(S+1)(3S^2+3S-1)]\ ,$$

where μ_B is the Bohr magneton, $\mathbf{S}$ the electronic spin ($S=\frac{5}{2}$) g the Lande tensor, A the hyperfine interaction tensor, $\mathbf{I}$ the nuclear spin ($I=\frac{5}{2}$ for ^{55}Mn), γ the nuclear gyromagnetic factor, and a the fine-structure constant related to the zero-field splitting by $W(\Gamma_8)-W(\Gamma_7)=3a$. The fine-structure term in S^4 has been written in the cubic axis system $\mathbf{x}\|[100]$, $\mathbf{y}\|[010]$, and $\mathbf{z}\|[001]$.

For Mn^{2+} in cubic ZnS, the electron paramagnetic resonance (EPR) parameters as measured by Schneider, Sircar, and Räuber[25] are $g=2.0024$ and $A=-64\times10^{-4}$ cm^{-1} for the isotropic tensors g and A in cubic symmetry, and $a=7.87\times10^{-4}$ cm^{-1} for the fine-structure constant.

Since the linewidths of 0.4 cm^{-1} observed in the optical spectra are about two orders of magnitude larger than the zero-field splitting $3a$, the fine-structure Hamiltonian can be safely neglected with respect to the Zeeman Hamiltonian in our optical experiments as soon as H is greater than 0.1 or 0.2 T; that is, as soon as a splitting of the states $\Gamma_6(^4E)$, $\Gamma_8(^4E)$, or $\Gamma_7(^4E)$ is observed.

The hyperfine structure of the fundamental state will not be observed in our optical experiments since the spacings AM_SM_I between two consecutive hyperfine structure lines associated with a state SM_S are at most 160×10^{-4} cm^{-1}, a value obtained for the states $|SM_S=+\frac{5}{2}\rangle$. Furthermore, the hyperfine structure will not contribute very significantly to the broadening of the optical transitions since, for example, the six hyperfine structure lines associated with states $|SM_S\rangle=+\frac{5}{2}\rangle$ extend to 0.08 cm^{-1}, a value which is five times less than the linewidth of the optical transitions.

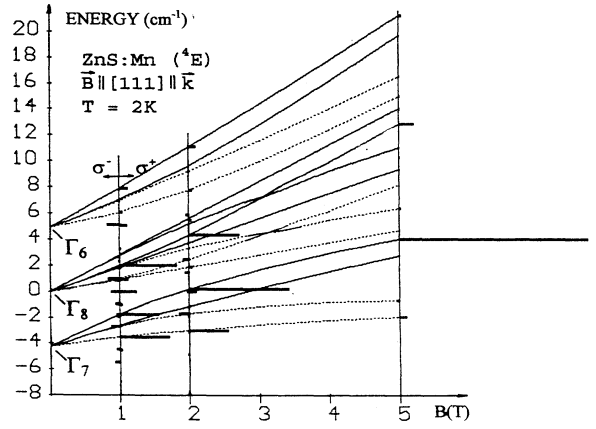

FIG. 5. Theoretical energy levels and dipole strengths in terms of the magnetic field. The solid and dotted lines correspond to transitions from the fundamental states $^6A_1$ ($M_S=-\frac{5}{2}$) and $^6A_1$ ($M_S=-\frac{3}{2}$), respectively. The relative dipole strengths for the polarizations σ^+ and σ^- are given for $B=1$, 2, and 5 T, and for all transitions to the fundamental state.

C. Polarization effects

Several perturbation schemes contribute to the dipole strength of the transition $^6A_1\rightarrow{}^4E$ The perturbation schemes depend on the chosen model, such as the crystal-field model, the covalent model, and the relativistic model. As we are primarily interested in the relative dipole strength (RDS) of the observed transitions, the RDS's will be given by symmetry considerations, thus avoiding the computation of the reduced matrix elements associated with perturbation schemes, which can be very difficult, particularly in the case of the covalent model.

In the crystal-field model, transition $^6A_1\rightarrow{}^4E$ is spin and parity forbidden, so that perturbation schemes involving the spin-orbit interaction, odd-parity configurations $3d^44p, 3d^44f$, etc., the odd part Hc_{odd} of the crystal field in symmetry T_d, and the electric dipole moment $\mathbf{M}$ will intervene in the calculation of the RDS.

In a molecular model, the relevant states are built, for example, from linear combinations of atomic orbitals of the electrons d of the metal and p of the ligands, so that the transitions $^6A_1\rightarrow{}^4E$ are spin forbidden but no longer parity forbidden in symmetry T_d.

In order to simply calculate the RDS in the crystal-field model, we can use the perturbation scheme whose relevant matrix elements are of the form

$$\langle {}^6A_1Jt\tau|H_{so}|{}^4T_{1k}J''t\tau\rangle\langle {}^4T_{1k}J''t\tau|H_{eq}|{}^4EJ't'\tau'\rangle\ ,$$

with

$$H_{\rm eq}=\sum_{^4E_{\rm odd}}\frac{M|^4E_{\rm odd}\rangle\langle^4E_{\rm odd}|H_{C\ \rm odd}}{W(3d^5)-W(^4E_{\rm odd})}+\sum_{^4T_{1\ \rm odd}}\frac{H_{C\ \rm odd}|^4T_{1\ \rm odd}\rangle\langle^4T_{1\ \rm odd}|M}{W(3d^5)-W(^4T_{1\ \rm odd})}\ .$$

In the first term of $H_{\rm eq}$, the dipole moment operator M of odd-parity relates the $^4T_1$ states of the fundamental configuration d^5 to the $^4E_{\rm odd}$ states of the excited odd-parity configurations. The $^4E_{\rm odd}$ states are related to the ^4E states of the fundamental configuration via the odd part $H_{C\ \rm odd}$ of the cubic crystal field of symmetry A_1. The second term can be interpreted in an analogous manner.

It can be shown that $H_{\rm eq}$ spans the representation T_d of T_d as does **M**. It is convenient to calculate the matrix elements in the spinor group T_d^* since all the relevant matrix elements involving $H_{\rm so}$ are identical, so that the matrix elements to calculate are those of the operators T_{20} and $T_{2\pm1}$ (see Table I).

In a magnetic field, each of the six fundamental states $i=0,1,2,\ldots,5$ as given by the diagonalization of the Zeeman Hamiltonian can be written as $\Sigma(^6A_1t\tau)i|^6A_1t\tau\rangle$. For the excited states, each of the eight states $j=a,b,\ldots,h$, as given by the diagonalization of the spin orbit and Zeeman Hamiltonians, are denoted $\Sigma(^4Et\tau)j|^4Et\tau\rangle$. By using the mixing parameters $(^6A_1t\tau)$ and $(^4Et\tau)$, the relative dipole strengths are given by

$$\sigma_k(i\rightarrow j)=\left|\left[\sum_{t\tau}(^6A_1t\tau)i^*\langle^6A_1t\tau|\right]\times(T_{2k})'\left[\sum_{t'\tau'}(^4Et'\tau')j|^4Et'\tau'\rangle\right]\right|^2,$$

with $k=0$ for polarization σ_π and $k=\pm1$ for polarizations $\sigma\pm$.

For $\mathbf{H}\|[111]$, the operators $(T_{2k})'$ are

$$(T_{20})'=(1/\sqrt{3})[T_{20}+(1+i)(1/\sqrt{2})T_{2-1}-(1-i)(1/\sqrt{2})T_{21}],$$

$$(T_{2\pm1})'=[1/(2\sqrt{3})][\pm2T_{20}+(\sqrt{3}\pm1)(1-i)(1/\sqrt{2})T_{21}+(\mp1+\sqrt{3})(1+i)(1/\sqrt{2})T_{2-1}].$$

The upper and lower signs correspond to the operators T_{2+1} and T_{2-1}, respectively.

The computation of the mixing parameters $(^6A_1t\tau)$ and $(^4Et\tau)$ has been performed in the cubic axis system $\mathbf{x}\|[100]$, $\mathbf{y}\|[010]$, and $\mathbf{z}\|001]$, which is the common axis system chosen for computing the energy levels and wave functions of the fundamental and excited states. The theoretical polarizations σ^+ and σ^- are represented in Fig. 5 for $H=1$, 2, and 5 T.

IV. COMPARISON WITH EXPERIMENTS AND DISCUSSION

The theoretical model has been compared in great detail to experimental results for $B=1$ T. Figure 6 shows that for this value of the magnetic field, the spectra σ^+ and σ^- consist of numerous and well-separated excitation lines, thus permitting a very detailed interpretation of these spectra. The Zeeman levels associated with lev-

TABLE I. Matrix elements of the operators T_{20}, T_{21}, and T_{2-1} intervening in the calculation of the relative dipole strengths defined in Sec. III.

	T_{20}			
	$(^4E)\Gamma_6\pm\frac{1}{2}$	$(^4E)\Gamma_7\pm\frac{1}{2}$	$(^4E)\Gamma_8\pm\frac{1}{2}$	$(^4E)\Gamma_8\mp\frac{3}{2}$
$(^6A_1)\Gamma_7\pm\frac{1}{2}$	$\mp\frac{1}{3\sqrt{2}}$	0	$-\frac{1}{3\sqrt{2}}$	0
$(^6A_1)\Gamma_8\pm\frac{1}{2}$	0	$\frac{1}{\sqrt{10}}$	0	$\pm\frac{1}{\sqrt{10}}$
$(^6A_1)\Gamma_8\mp\frac{3}{2}$	$\frac{1}{3\sqrt{10}}$	0	$\pm\frac{1}{3\sqrt{10}}$	0

	$T_{2\pm1}$							
	$(^4E)\Gamma_6\pm\frac{1}{2}$	$(^4E)\Gamma_6\mp\frac{1}{2}$	$(^4E)\Gamma_7\pm\frac{1}{2}$	$(^4E)\Gamma_7\mp\frac{1}{2}$	$(^4E)\Gamma_8\pm\frac{3}{2}$	$(^4E)\Gamma_8\pm\frac{1}{2}$	$(^4E)\Gamma_8\mp\frac{1}{2}$	$(^4E)\Gamma_8\mp\frac{3}{2}$
$(^6A_1)\Gamma_7\pm\frac{1}{2}$	0	$\pm\frac{1}{3}$	0	0	0	0	$\frac{1}{6}$	0
$(^6A_1)\Gamma_7\mp\frac{1}{2}$	0	0	0	0	0	0	0	$\frac{1}{2\sqrt{3}}$
$(^6A_1)\Gamma_8\pm\frac{3}{2}$	0	0	$\frac{\sqrt{3}}{2\sqrt{5}}$	0	0	0	0	$\mp\frac{1}{\sqrt{15}}$
$(^6A_1)\Gamma_8\pm\frac{1}{2}$	0	0	0	$\frac{1}{2\sqrt{5}}$	0	0	0	0
$(^6A_1)\Gamma_8\mp\frac{1}{2}$	$-\frac{1}{2\sqrt{15}}$	0	0	0	0	$\pm\frac{1}{\sqrt{15}}$	0	0
$(^6A_1)\Gamma_8\mp\frac{3}{2}$	0	$\frac{1}{6\sqrt{5}}$	0	0	0	0	$\mp\frac{2}{3\sqrt{5}}$	0

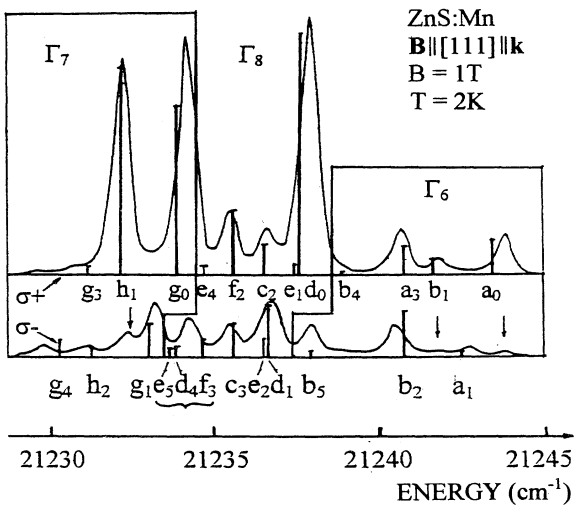

FIG. 6. Detailed analysis of the Zeeman spectra for $B=1$ T. The lines associated with states $\Gamma_6(^4E)$ and $\Gamma_7(^4E)$ are given in the insets, and the other lines are associated with the state $\Gamma_8(^4E)$. The vertical lines give the energies and relative dipole strengths for $T=2$ K as given by the theoretical model presented in Sec. III. Thermalization in the fundamental $^6A_1$ state has been taken into account. For the polarization σ^+ all experimental lines have been recognized unambiguously. For the polarization σ^-, the transitions $e5$, $d4$, and $f3$ cannot be unambiguously associated with the experimental line at 21 234.25 cm^{-1}. The lines marked by an arrow are interpreted in Sec. IV.

els Γ_6, Γ_7, and Γ_8 will be analyzed because, as it will be shown, the indexation given in Fig. 3 cannot give the nature of all observed liens for all values of the magnetic field.

The Zeeman levels associated with Γ_6 are shown in an inset in Fig. 6. For the polarization σ^+ three prominent lines are associated with the transitions $a0$, $b1$, and $a3$, and the weak line is associated with transition $b4$. For the polarization σ^-, three lines are associated with transitions $a1$, $b2$, and $b5$. It must be noted that the computed and experimental energies are slightly different, the difference being at most 0.4 cm^{-1} for transition $a0$. Transitions $b0$, $a2$, and $a4$ have not been associated with observed transitions, since their dipole strengths are predicted to be zero by the theoretical model. In spectra σ^-, two lines marked by an arrow in the inset denoted Γ_6 are not given by the theoretical model; their origin will be discussed below.

The Zeeman levels associated with Γ_7 are $g0$, $h1$, and $g3$ for polarization σ^+, and with $g1$, $h2$, and $g4$ for polarization σ^- (see Fig. 6). Line $h0$, whose theoretical amplitude is zero has not been attributed to an experimental line. The theoretical and experimental energies differ by at most 0.4 cm^{-1} for line $g4$. For polarization σ^-, the origin of the line marked by an arrow in the inset denoted Γ_7 will be studied below.

The Zeeman levels associated with Γ_8 are $d0$, $e1$, $c2$, $f2$, and $e4$ for polarization σ^+. For polarization σ^-, two lines can be safely associated with the three Zeeman levels $d1$, $e2$, and $c3$, since levels $d1$ and $e2$ are almost degenerate. Only one line appears at 21 234.25 cm^{-1} where three Zeeman levels $f3$, $d4$, and $e5$ are expected.

By considering the overall spectrum for polarization σ^+, we can note the good agreement between the experimental and theoretical energy levels, which differ by at most 0.4 cm^{-1} for line $a0$; 0.3 cm^{-1} for the lines $d0$, $g0$, and $g3$; and 0.2 cm^{-1} for the other lines. The dipole strengths are in excellent agreement for all lines except for the line $g0$; in fact, RDS's of $d0$ and $g0$ are very sensitive to the temperature, as has been checked by calculating the dipole strengths at 1.9 K.

For polarization σ^-, almost all lines have been unambiguously associated with Zeeman levels. The origin of the three lines marked by an arrow and the precision of the experiments will now be discussed.

The first hypothesis is that there exists a slight misorientation of the magnetic field or of the wave vector **k** with respect to the chosen [111] axis of the crystal, thus allowing the appearance of additional lines in the experimental spectra. This hypothesis could also explain the slight shift of the experimental lines with respect to the theoretical positions. Following this hypothesis, the three lines marked by an arrow in Fig. 6 are associated with the Zeeman levels $a0$, $b1$, and $h1$, since no other lines are expected in the energy-level diagram. Calculations of the energy levels and RDS's were performed by introducing slight disorientations of **B** with respect to the [111] axis of the crystal. It was found that a misorientation of approximately 1° permits us to interpret all experimental lines.

Another hypothesis is that the slight shifts of the experimental lines and the slight variations of the dipole strengths are due to the term in $\mathbf{L}\cdot\mathbf{H}$ in the Zeeman Hamiltonian. Finally, the degree of polarization, although better than 95%, could also account for the variations of the dipole strengths but not for the shifts of the lines. Since the samples used in the Zeeman experiments have parallel {111} faces, effects due to refraction or internal depolarization seem to be very unlikely.

Of course, weak lines which are not predicted by the theoretical model for the RDS's also appear for other values of the magnetic field. For example, for $B=5$ T, five transitions appear in the spectra σ^-, while only one transition $g0$ with a non-negligible amplitude is expected from the theoretical model (see Fig. 5). The other four transitions are associated with Zeeman levels appearing at the same energies in the σ^+ spectra. Six transitions $a0$, $d0$, $e0$, $g0$, $h0$, and $h1$ appear in the spectra σ^+ represented in Fig. 2(b); the energies and the RDS's of the transitions $a0$, $d0$, $g0$, and $h1$ are in very good agreement with the theoretical values, while the theoretical RDS's of the transitions $e0$ and $h0$ are predicted to be zero. Other very weak transitions which cannot be represented in Fig. 2(b) appear in the experimental spectra, and are correctly predicted by the theoretical model for the energies.

V. CONCLUSION

A very detailed analysis of the Zeeman effect on the ^4E state of Mn^{+2} in ZnS has shown that all observed excita-

tion lines are transitions from the fundamental states $|^6A_1, M_S=-\frac{5}{2}, -\frac{3}{2}, -\frac{1}{2}, +\frac{1}{2}, +\frac{3}{2}$, and $\frac{5}{2}\rangle$ to the Zeeman states, except the state $|\Gamma_8 c\rangle$, of the multiplet ^4E. It has been shown that the energies of the experimental lines are very well predicted by the Zeeman Hamiltonian $g_e\mu_B \mathbf{H}\cdot\mathbf{S}$, the difference between the theoretical and experimental energies being less than 0.4 cm^{-1} for all analyzed lines.

In what concerns the RDS's, several lines whose amplitudes were predicted to be zero by the theoretical model have been observed. The presence of these lines has been interpreted as being due to a slight misorientation of the magnetic field or the wave vector with respect to the [111] axis of the crystal, the degree of polarization of the experimental setup, and eventually the influence of the term in $\mathbf{L}\cdot\mathbf{H}$ of the Zeeman Hamiltonian. In fact, the crystal-field model predicts that the second-order contribution of the term in $\mathbf{L}\cdot\mathbf{H}$ is approximately 20 times smaller than the first-order contribution of the term in $\mathbf{L}\cdot\mathbf{S}$. However, covalency could have increased the importance of the term in $\mathbf{L}\cdot\mathbf{H}$ since the molecular spin-orbit interaction intervenes in the perturbation scheme. Finally, we can note that no indication has been obtained concerning the coupling between the states $|(^4A_1)\Gamma_8\rangle$ and $|(^4E)\Gamma_8\rangle$.

ACKNOWLEDGMENT

We would like to thank J. Mahrt for cooperation during the development of the experimental setup.

[1]For reviews and analyses of the electronic and vibronic structures of d^n ions see, for example, M. D. Sturge, in *Solid State Physics,* edited by F. Seitz and G. Turnbull (Academic, New York, 1967), Vol. 20; A. Abragam and B. Bleaney, *Electron Paramagnetic Resonance of Transition Ions* (Clarendon, Oxford, 1969); S. Sugano, Y. Tanabe, and H. Kamimura, *Multiplets of Transition Metal Ions* (Academic, New York, 1970); F. S. Ham, in *Electron Paramagentic Resonance,* edited by S. Geschwind (Plenum, New York 1972); R. Engleman, *The Jahn-Teller Effect in Molecules and Crystals* (Wiley, New York, 1972).

[2]L. E. Orgel, J. Chem. Phys. **23**, 1004 (1955).

[3]S. Sugano and Y. Tanabe, J. Phys. Soc. Jpn. **9**, 753 (1954); **9**, 766 (1954).

[4]S. Koide and M. H. L. Pryce, Philos. Mag. **3**, 607 (1958).

[5]Molecular-orbital theories have been developed, for example, by A. D. Liehr and C. J. Ballhausen, Phys. Rev. **106**, 1161 (1957); C. J. Ballhausen and H. B. Gray, *Molecular Orbital Theory* (Benjamin, New York, 1965); L. L. Lohr, Jr., J. Chem. Phys. **45**, 3611 (1966).

[6]Simplified semiempirical covalent models have been elaborated by D. Curie, C. Barthou, and B. Canny, J. Chem. Phys. **61**, 3048 (1974); A. J. O'Neill and J. W. Allen, Solid State Commun. **46**, 833 (1983); S. W. Berniacki, Phys. Status Solidi B **118**, 525 (1983); **131**, 349 (1985); **132**, 557 (1985); A. Fazzio, M. J. Caldas, and A. Zunger, Phys. Rev. B **30**, 3430 (1984); A. Zunger, in *Solid State Physics,* edited by H. Ehrenreich and D. Turnbull (Academic, New York, 1986), Vol. 39, p. 275.

[7]D. Fournier, A. C. Boccara, and J. C. Rivoal, J. Phys. C **10**, 113 (1977).

[8]R. Parrot, C. Naud, C. Porte, D. Fournier, A. C. Boccara, and J. C. Rivoal, Phys. Rev. B **17**, 1057 (1978).

[9]P. Koidl, Phys. Status Solidi **74**, 477 (1976).

[10]G. Hofman, F. G. Anderson, and J. Weber, Phys. Rev. B **47**, 9711 (1991).

[11]R. Parrot, C. Naud, and F. Gendron, Phys. Rev. B **13**, 3748 (1976).

[12]R. Parrot and C. Blanchard, Phys. Rev. B **6**, 3992 (1972).

[13]R. Parrot, C. Naud, F. Gendron, C. Porte, and M. Lemercier, J. Chem. Phys. **85**, 4932 (1986).

[14]C. Naud, C. Porte, F. Gendron, and R. Parrot, Phys. Rev. B **20**, 3333 (1979).

[15]H. Watanabe, *Operator Methods in Ligand Field Theory* (Prentice-Hall, Englewood Cliffs, NJ, 1966).

[16]A. Landi, A. Deville, and R. Ranvaud, J. Phys. (Paris) **41**, 161 (1980).

[17]C. Blanchard, A. Landi, R. Parrot, and C. Naud, J. Lumin. **9**, 329 (1974).

[18]J. Schulze and H. E. Gumlich, J. Cryst. Growth **59**, 347 (1982).

[19]The optical spectra of Mn^{2+} in ZnS with stacking faults have been described in detail by R. Parrot, A. Geoffroy, C. Naud, W. Busse, and H. E. Gumlich, Phys. Rev. B **23**, 5288 (1981); U. W. Pohl, A. Ostermeier, W. Busse, and H. E. Gumlich, *ibid.* **42**, 5751 (1990).

[20]The optical spectra of Mn-Mn pairs have been analyzed by U. W. Pohl and H. E. Gumlich, Phys. Rev. B **40**, 1194 (1989).

[21]J. Fergusson, E. R. Krausz, and H. J. Guggenheim, Mol. Phys. **27**, 577 (1974).

[22]W. C. Egbert, P. M. Selzer, and W. M. Yen, Appl. Opt. **15**, 1158 (1976).

[23]J. S. Griffith, *The Irreducible Tensor Method for Molecular Symmetry Groups* (Prentice-Hall, Englewood Cliffs, NJ, 1962).

[24]J. S. Griffith, *The Theory of Transition Metal Ions* (Cambridge University Press, London, 1971).

[25]J. Schneider, S. R. Sircar, and A. Räuber, Z. Naturforsch. **18a**, 980 (1963).